Journal of Sound and Vibration (1995) **181**(2), 261–278

DYNAMICS OF FLEXIBLE BEAMS UNDERGOING OVERALL MOTIONS

H. H. Yoo

Department of Mechanical Design and Production Engineering, *Hanyang University*, *Haengdang-Dong* 17, *Sungdong-Gu*, *Seoul*, *Korea*, 133-791

R. R. Ryan

Mechanical Dynamics, *Inc.*, 2301 *Commonwealth Boulevard*, *Ann Arbor*, *Michigan* 48105, *U.S.A.*

AND

R. A. Scott

Department of Mechanical Engineering and Applied Mechanics, *The University of Michigan at Ann Arbor*, *Michigan* 48109, *U.S.A.*

(*Received* 19 *April* 1993, *and in final form* 4 *January* 1994)

A modelling method for straight beams undergoing large overall motions as well as small elastic deformations is presented in this paper. Different from the classical linear Cartesian modelling method which employs three Cartesian deformation variables, the present modelling method uses a non-Cartesian variable along with two Cartesian variables to describe the elastic deformation. A quadratic form of the strain energy expressed with the hybrid set of deformation variables is used to obtain the generalized active forces and a geometric constraint equation relating the non-Cartesian variable and Cartesian variables is used to obtain the generalized inertia forces in the equations of motion. The present modelling method not only provides accurate simulation results but also clarifies the limit of validity of the classical linear Cartesian modelling method.

1. INTRODUCTION

A dynamic modelling method is presented for straight beams undergoing large overall motions as well as small strain elastic deformations. Flexible structures are often idealized as beams and their dynamic characteristics are represented by those of beams. Large overall motions consist of translational and rotational motions. They are frequently called rigid body motions. There are several engineering examples which have beam-like shapes and undergo large overall motions. Satellite antennas and helicopter blades are such examples. Engineering examples of flexible structures will appear more frequently, since the general structural design trend is toward lighter systems with increasingly faster dynamic response and minimal power requirements.

Structural flexibility can cause problems for the standard operational motions of a system. For instance, in 1958 the Explorer I spacecraft experienced a radical instability, which was blamed on energy dissipation induced by the vibration of long antennas of the satellite [1]. To avoid this kind of problem, the dynamic characteristics of structure should be identified accurately so that one can properly design or control the system.

The first modelling approach for beams, which hereafter will be referred to as the C.L.C. (classical linear Cartesian) approach, was introduced [2, 3] in the 1970s when the speed of

0022–460X/95/120261 + 18 $08.00/0

computer and numerical methods was progressing rapidly. This approach is based on the classical linear elastic modelling, where geometric as well as material linearity is assumed. It has merits such as simplicity of formulation, ease of implementation in finite element methods, and available co-ordinate reduction techniques [4], which are often critically important for dynamic analyses of structures. Because of these merits, the C.L.C. approach has been widely used by many engineers. However, this approach displays a critical flaw when the structures undergo large overall rotational motions. In this case, the approach produces erroneous results in numerical simulations.

To resolve the problem of the C.L.C. approach, several non-linear methods [5–8] have been introduced. Since the problem is believed to originate from the assumption of geometric linearity, those methods are based on geometric non-linear relations between strains and displacements. With the non-linear methods, the accuracy problem was shown to be resolved. However, other problems were raised due to the non-linearity of the modelling methods. Actually, these modelling methods lack the merits of the C.L.C. approach, including the capability of co-ordinate reduction. Without this capability, a large amount of computational effort is needed for dynamic analyses. Furthermore, a question still remains for the C.L.C. approach: Exactly under what conditions does the approach fail? If one knows the answer, one does not have to rely all the time on the inefficient non-linear approach.

The purposes of this paper are to overcome the disadvantage of the non-linear approach and to identify explicitly the limit of validity of the C.L.C. approach. The present work is based on the work in reference [9]. Compared to the work in reference [9], the present work simplifies the procedure of formulating the derivation of the equations of motion, clarifies its relation to non-linear modelling, provides a simple explanation of the modelling effectiveness, and presents more numerical examples, including a three-dimensional one.

In the following sections, the procedure for deriving the equations of motion is described. To focus on the effect of large overall motions on the elastic behavior of flexible beams, large overall motions are prescribed. Numerical examples show the importance of the effect. In the penultimate section, a simple discrete example is introduced. The discrete system is designed to be analogous to a rotating beam so that critical physical phenomena involved in the beam can be easily understood through the system.

2. SYSTEM AND VARIABLE DESCRIPTION

The following assumptions are made. The beam has homogeneous and isotropic material properties. The elastic and centroidal axes in the cross-section of the beam coincide so that no eccentricity effect needs to be considered. The beam has a slender shape so that shear and rotary inertia effects are neglected. Large overall motions are prescribed as functions of time. No external forces are given in the system of concern. These assumptions are made to simplify the formulation and to focus on the critical effects induced by large overall motions which make differences between the C.L.C. and the present modelling methods. However, they can be removed without having many difficulties if necessary. Such cases have been well described in reference [10].

In Figure 1 are shown the configurations of a straight beam before and after deformation. The deformation can be represented by three scalar variables in 3-D space. Conventionally, Cartesian variables, as shown in the figure, are widely used. They are used in the C.L.C. modelling method. In the present modelling method, a non-Cartesian variable along with two Cartesian variables is used instead of three Cartesian variables. s, denoting the arc length stretch, is used instead of u_1, which denotes the Cartesian distance measure of a generic point in the axial direction of the undeformed configuration.

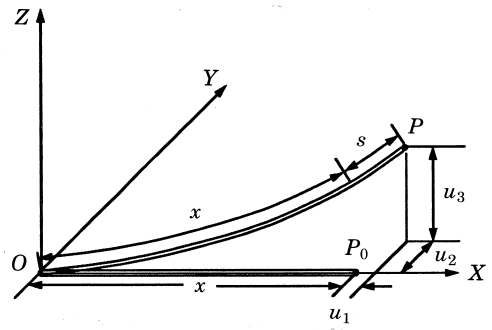

Figure 1. The configuration of a beam before and after deformation.

u_2 and u_3, which denote the lateral displacements, are also used in the present modelling method.

There is a geometric relation between the arc length stretch s and the Cartesian variables. This relation is later used to derive generalized inertia forces in the equations of motion. In reference [9], the relation is given as

$$x + s = \int_0^{x+u_1} \left[1 + \left(\frac{\partial u_2}{\partial \sigma}\right)^2 + \left(\frac{\partial u_3}{\partial \sigma}\right)^2\right]^{1/2} \mathrm{d}\sigma. \tag{1}$$

In words, this equation expresses the fact that the arc length distance from the reference point O of the beam B to some generic particle P of the beam can be expressed as either (1) the sum of the distance x (from the reference point O to the undeformed position of a generic point P_0) and the neutral axis stretch s, or (2) the integral, from zero to $x + u_1$ of a differential arc length of the beam. This formulation has analytical and numerical difficulties associated with it: namely, the determination of u_1. The explicit dependence of the integral on u_1 complicates the procedure of deriving the equations of motion and makes it difficult to obtain the numerical value of u_1. In the present work, a different strategy is adopted to attack the difficulties. The drawbacks of the form presented in equation (1) can be overcome by changing the domain of integration to include only the undeformed length instead of the deformed length and altering the integrand accordingly. Thus, as an equivalent to equation (1), one can write

$$x + s = \int_0^{x} \left[\left(1 + \frac{\partial u_1}{\partial \sigma}\right)^2 + \left(\frac{\partial u_2}{\partial \sigma}\right)^2 + \left(\frac{\partial u_3}{\partial \sigma}\right)^2\right]^{1/2} \mathrm{d}\sigma \tag{2}$$

and, by using a binomial expansion of the integrand of equation (2), this can be shown to give

$$s = u_1 + \tfrac{1}{2} \int_0^{x} \left[\left(\frac{\partial u_2}{\partial \sigma}\right)^2 + \left(\frac{\partial u_3}{\partial \sigma}\right)^2\right] \mathrm{d}\sigma + (\text{higher order terms}). \tag{3}$$

One of the eventual goals of the present modelling method is the development of equations of motion which are *linear* in the deformation variables s, u_2 and u_3. Therefore, it seems sensible to search for an approximate form of s which will yield only those linear and quadratic terms appearing explicitly in equation (3). Such an approximate form is

$$s = u_1 + \tfrac{1}{2} \int_0^{x} \left[\left(\frac{\partial u_2}{\partial \sigma}\right)^2 + \left(\frac{\partial u_3}{\partial \sigma}\right)^2\right] \mathrm{d}\sigma. \tag{4}$$

Differentiation of this expression for s with respect to x yields

$$\frac{\partial s}{\partial x} = \left(\frac{\partial u_1}{\partial x}\right) + \tfrac{1}{2}\left[\left(\frac{\partial u_2}{\partial x}\right)^2 + \left(\frac{\partial u_3}{\partial x}\right)^2\right]. \tag{5}$$

This equation shows that the differentiation of the approximate s is equivalent to the well known von Kármán strain measure for beams. Actually, without any approximation, $\partial s/\partial x$ represents the exact strain for the stretching of a beam. The use of equation (4) not only simplifies the derivation of the equations of motion but also provides a simple way of determining u_1 numerically when the variables s, u_2 and u_3 are known.

3. APPROXIMATION AND STRAIN ENERGY

In the previous section, it was mentioned that the deformation variables, s, u_2 and u_3 are used in the present modelling method. This implies that these continuous variables should be approximated by using spatial functions and corresponding coordinates to derive the ordinary differential equations of motion. In the present work, the Rayleigh–Ritz method is used to approximate the variables as follows:

$$s(x, t) = \sum_{j=1}^{\mu} \phi_{1j}(x) q_j(t), \qquad u_2(x, t) = \sum_{j=1}^{\mu} \phi_{2j}(x) q_j(t), \qquad u_3(x, t) = \sum_{j=1}^{\mu} \phi_{3j}(x) q_j(t). \tag{6–8}$$

Here ϕ_{1j}, ϕ_{2j} and ϕ_{3j} are the spatial functions. These functions can be obtained from the vibration analysis of the beam undergoing no rigid body motion. ϕ_{1j} is the modal function of the longitudinal vibration, and ϕ_{2j} and ϕ_{3j} are modal functions of the bending vibrations in the two lateral directions. The q_js are generalized co-ordinates and μ is the total number of modal co-ordinates. The same modal functions are often used for u_1, u_2, and u_3 in the C.L.C. modelling method. For the convenience of the formalism, s, u_2 and u_3 explicitly have the same number of co-ordinates μ. However, they are not actually coupled. For instance, ϕ_{1j} is not zero only if $j \leqslant \mu_1$, ϕ_{2j} is not zero only if $\mu_1 < j \leqslant \mu_1 + \mu_2$ and ϕ_{3j} is not zero only if $\mu_1 + \mu_2 < j \leqslant \mu_1 + \mu_2 + \mu_3$. In other words, μ_1, μ_2 and μ_3 denote the actual numbers of generalized co-ordinates for s, u_2 and u_3, respectively. μ is the total sum of μ_1, μ_2 and μ_3.

In the C.L.C. modelling method, u_1 (instead of s in equation (6)) is approximated and the strain energy expression is

$$U = \tfrac{1}{2}\int_0^L EA\left(\frac{\partial u_1}{\partial x}\right)^2 \mathrm{d}x + \tfrac{1}{2}\int_0^L EI_{zz}\left(\frac{\partial^2 u_2}{\partial x^2}\right)^2 \mathrm{d}x + \tfrac{1}{2}\int_0^L EI_{yy}\left(\frac{\partial^2 u_3}{\partial x^2}\right)^2 \mathrm{d}x, \tag{9}$$

where E denotes Young's modulus, A is the cross-sectional area of the beam, I_{zz} and I_{yy} are the second area moments of the cross-section, and L is the undeformed length of the beam. For the present modelling method, however, the following strain energy expression is used:

$$U = \tfrac{1}{2}\int_0^L EA\left(\frac{\partial s}{\partial x}\right)^2 \mathrm{d}x + \tfrac{1}{2}\int_0^L EI_{zz}\left(\frac{\partial^2 u_2}{\partial x^2}\right)^2 \mathrm{d}x + \tfrac{1}{2}\int_0^L EI_{yy}\left(\frac{\partial^2 u_3}{\partial x^2}\right)^2 \mathrm{d}x. \tag{10}$$

Equations (9) and (10) differ only in their first terms, which represent the stretching energy of the beam. Since s represents the exact stretch of the beam, the first term of equation (10) represents the exact stretching energy of the beam. On the other hand, since $\partial u_1/\partial x$ of equation (9) is the linear approximation of $\partial s/\partial x$, the first term of equation (9) does not represent the exact stretching energy. With the three Cartesian variables, the exact

stretching energy can be expressed in a non-quadratic form which results in non-linear active forces in the equations of motion. Actually, this is how the non-linear modelling methods in references [6] and [7] express the strain energy forms. For example, if the right side of equation (5), which is the approximation of $\partial s/\partial x$, is substituted into equation (10), one can obtain the strain energy expression based on the von Kármán strain measure, which results in non-linear generalized active force terms. On the other hand, with the quadratic form of strain energy given in equation (10), the generalized active force terms become linear and the exact stretching energy can be considered. However, the use of s complicates the formulation of generalized inertia forces in the equations of motion and results in non-linear generalized inertia force terms. The non-linear inertia force terms are linearized to obtain the final equations of motion for the present modelling method.

4. EQUATIONS OF MOTION

In the present section, Kane's method is employed to derive the equations of motion. This method provides a direct and systematic way of deriving ordinary differential equations of motion for continua such as beams, plates and shells. With the assumptions given in section 2, the equations of motion can be obtained for beams as follows:

$$\int_0^L \rho\left(\frac{\partial \vec{v}^P}{\partial \dot{q}_i}\right)\cdot \vec{a}^P \,\mathrm{d}x + \frac{\partial U}{\partial q_i} = 0, \qquad i = 1, \ldots, \mu. \tag{11}$$

ρ is the mass per unit length of the beam, the $\dot{q}_i$s are the time derivatives of the generalized co-ordinates, and $\vec{v}^P$ and $\vec{a}^P$ are the inertial velocity and acceleration of the center point P of a differential element of the beam (see Figure 2). The acceleration can be obtained simply by differentiating the expression for the inertial velocity,

$$\vec{v}^P = \vec{v}^O + \vec{\omega}^A \times (\vec{r} + \vec{u}) + {}^A\vec{v}^P, \tag{12}$$

where O is a reference point identifying a point fixed in a floating frame A in the system, $\vec{v}^O$ is the inertial velocity of point O, $\vec{\omega}^A$ is the inertial angular velocity of the floating reference frame, $\vec{r}$ is a position vector from O to the location of P in the undeformed body, $\vec{u}$ is the displacement vector of point P, and ${}^A\vec{v}^P$ is the relative velocity of P in frame A obtained by taking the time derivative of $\vec{u}$ in frame A. In component notation, the various terms can be written as

$$\vec{r} = x\vec{a}_1, \qquad \vec{u} = u_1\vec{a}_1 + u_2\vec{a}_2 + u_3\vec{a}_3 \tag{13, 14}$$

$$\vec{v}^O = v_1\vec{a}_1 + v_2\vec{a}_2 + v_3\vec{a}_3, \qquad \vec{\omega}^A = \omega_1\vec{a}_1 + \omega_2\vec{a}_2 + \omega_3\vec{a}_3. \tag{15, 16}$$

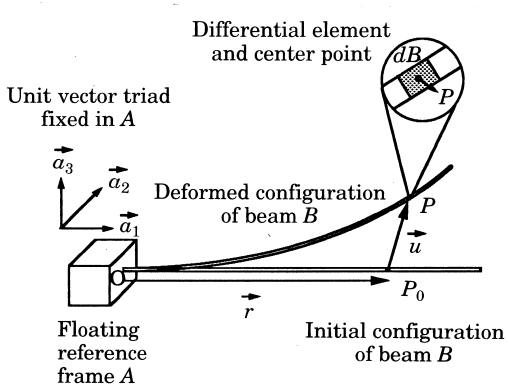

Figure 2. The kinematics of a beam undergoing large overall motion.

By using equations (4), (6)–(8) and (13)–(16), the partial derivative of the velocity of P with respect to the generalized speed $\dot{q}_i$ can be obtained as

$$\frac{\partial \vec{v}^P}{\partial \dot{q}_i} = \left[\phi_{1i} - \sum_{j=1}^{\mu} \left(\int_0^x \phi_{2i,\eta} \phi_{2j,\eta} \, \mathrm{d}\eta \right) q_j - \sum_{j=1}^{\mu} \left(\int_0^x \phi_{3i,\eta} \phi_{3j,\eta} \, \mathrm{d}\eta \right) q_j \right] \vec{a}_1 + \phi_{2i} \vec{a}_2 + \phi_{3i} \vec{a}_3, \tag{17}$$

where η denotes partial differentiation with respect to the dummy spatial variable η. Non-linear equations of motion can be derived from equation (11) by using equation (17), along with the expression for the system strain energy and the acceleration of P. The final procedure in the present modelling method is to linearize the equations with respect to the generalized co-ordinates for the elastic deformations s, u_2 and u_3. The results are described in equations (18)–(20), which will be presented in what follows. The whole procedure is straightforward except for the use of the integration by parts technique employed to obtain some motion-induced stiffness terms in the equations of motion. Those terms appear in the second and third lines of equations (19) and (20). If the terms are deleted, the resulting equations become equivalent to those of the C.L.C. modelling method. Equations (18)–(20) are as follows:

$$\begin{aligned}
&\sum_{j=1}^{\mu} \left[\left(\int_0^L \rho \phi_{1i} \phi_{1j} \, \mathrm{d}x \right) \ddot{q}_j - (\omega_2^2 + \omega_3^2) \left(\int_0^L \rho \phi_{1i} \phi_{1j} \, \mathrm{d}x \right) q_j + \left(\int_0^L EA \phi_{1i,x} \phi_{1j,x} \, \mathrm{d}x \right) q_j \right] \\
&\quad - \sum_{j=1}^{\mu} \left[2\omega_3 \left(\int_0^L \rho \phi_{1i} \phi_{2j} \, \mathrm{d}x \right) \dot{q}_j - (\omega_1 \omega_2 - \dot{\omega}_3) \left(\int_0^L \rho \phi_{1i} \phi_{2j} \, \mathrm{d}x \right) q_j \right] \\
&\quad + \sum_{j=1}^{\mu} \left[2\omega_2 \left(\int_0^L \rho \phi_{1i} \phi_{3j} \, \mathrm{d}x \right) \dot{q}_j + (\omega_1 \omega_3 + \dot{\omega}_2) \left(\int_0^L \rho \phi_{1i} \phi_{3j} \, \mathrm{d}x \right) q_j \right] \\
&= (\omega_2^2 + \omega_3^2) \int_0^L \rho x \phi_{1i} \, \mathrm{d}x - (\dot{v}_1 + \omega_2 v_3 - \omega_3 v_2) \int_0^L \rho \phi_{1i} \, \mathrm{d}x;
\end{aligned} \tag{18}$$

$$\begin{aligned}
&\sum_{j=1}^{\mu} \left[\left(\int_0^L \rho \phi_{2i} \phi_{2j} \, \mathrm{d}x \right) \ddot{q}_j - (\omega_1^2 + \omega_3^2) \left(\int_0^L \rho \phi_{2i} \phi_{2j} \, \mathrm{d}x \right) q_j + \left(\int_0^L EI_{zz} \phi_{2i,xx} \phi_{2j,xx} \, \mathrm{d}x \right) q_j \right] \\
&\quad - \sum_{j=1}^{\mu} \left[(\dot{v}_1 + \omega_2 v_3 - \omega_3 v_2) \left(\int_0^L \rho (L - x) \phi_{2i,x} \phi_{2j,x} \, \mathrm{d}x \right) q_j \right] \\
&\quad + \sum_{j=1}^{\mu} \left[(\omega_2^2 + \omega_3^2) \left(\int_0^L \frac{\rho}{2} (L^2 - x^2) \phi_{2i,x} \phi_{2j,x} \, \mathrm{d}x \right) q_j \right] \\
&\quad - \sum_{j=1}^{\mu} \left[2\omega_1 \left(\int_0^L \rho \phi_{2i} \phi_{3j} \, \mathrm{d}x \right) \dot{q}_j - (\omega_2 \omega_3 - \dot{\omega}_1) \left(\int_0^L \rho \phi_{2i} \phi_{3j} \, \mathrm{d}x \right) q_j \right] \\
&\quad + \sum_{j=1}^{\mu} \left[2\omega_3 \left(\int_0^L \rho \phi_{2i} \phi_{1j} \, \mathrm{d}x \right) \dot{q}_j + (\omega_1 \omega_2 + \dot{\omega}_3) \left(\int_0^L \rho \phi_{2i} \phi_{1j} \, \mathrm{d}x \right) q_j \right] \\
&= -(\omega_1 \omega_2 + \dot{\omega}_3) \int_0^L \rho x \phi_{2i} \, \mathrm{d}x - (\dot{v}_2 + \omega_3 v_1 - \omega_1 v_3) \int_0^L \rho \phi_{2i} \, \mathrm{d}x;
\end{aligned} \tag{19}$$

$$\sum_{j=1}^{\mu}\left[\left(\int_0^L \rho\phi_{3i}\phi_{3j}\,\mathrm{d}x\right)\ddot{q}_j - (\omega_1^2+\omega_2^2)\left(\int_0^L \rho\phi_{3i}\phi_{3j}\,\mathrm{d}x\right)q_j + \left(\int_0^L EI_{yy}\phi_{3i,xx}\phi_{3j,xx}\,\mathrm{d}x\right)q_j\right]$$

$$-\sum_{j=1}^{\mu}\left[(\dot{v}_1+\omega_2 v_3-\omega_3 v_2)\left(\int_0^L \rho(L-x)\phi_{3i,x}\phi_{3j,x}\,\mathrm{d}x\right)q_j\right]$$

$$+\sum_{j=1}^{\mu}\left[(\omega_2^2+\omega_3^2)\left(\int_0^L \frac{\rho}{2}(L^2-x^2)\phi_{3i,x}\phi_{3j,x}\,\mathrm{d}x\right)q_j\right]$$

$$-\sum_{j=1}^{\mu}\left[2\omega_2\left(\int_0^L \rho\phi_{3i}\phi_{1j}\,\mathrm{d}x\right)\dot{q}_j - (\omega_1\omega_3-\dot{\omega}_2)\left(\int_0^L \rho\phi_{3i}\phi_{1j}\,\mathrm{d}x\right)q_j\right]$$

$$+\sum_{j=1}^{\mu}\left[2\omega_1\left(\int_0^L \rho\phi_{3i}\phi_{2j}\,\mathrm{d}x\right)\dot{q}_j + (\omega_2\omega_3+\dot{\omega}_1)\left(\int_0^L \rho\phi_{3i}\phi_{2j}\,\mathrm{d}x\right)q_j\right]$$

$$= -(\omega_1\omega_3-\dot{\omega}_2)\int_0^L \rho x\phi_{3i}\,\mathrm{d}x - (\dot{v}_3+\omega_1 v_2-\omega_2 v_1)\int_0^L \rho\phi_{3i}\,\mathrm{d}x. \tag{20}$$

One of the merits of the present modelling method is that it gives a clear indication of the factors involved in motion-induced stiffness variations. For example, as one may see from the second and third terms in square brackets of equations (19) and (20), $(\dot{v}_1+\omega_2 v_3-\omega_3 v_2)$ and $(\omega_2^2+\omega_3^2)$ are the overall motions involved in the stiffness variations. Such overall motion terms do not appear in any non-linear modelling methods (see references [5, 6]). Instead, such effects are compensated by non-linear elastic force terms in the non-linear modelling methods. However, in the C.L.C. modelling method, neither the overall motion terms nor non-linear elastic force terms appear in the equations of motion. As such overall motion terms become significant for the system, those terms should be included to obtain accurate system responses. However, if the overall motion terms are not significant to the system, the C.L.C. modelling method can be used without any trouble. In other words, by inspecting the explicit factors discussed above, one may easily determine whether or not the C.L.C. modelling method can be safely used.

5. NUMERICAL EXAMPLES

A cantilever beam attached to a rigid base is shown in Figure 3. The base performs a planar rotational motion around the vertical axis which is given as

$$\Omega = \begin{Bmatrix} \Omega_s[6\tau^5-15\tau^4+10\tau^3] & \text{if } 0\leqslant\tau\leqslant 1 \\ \Omega_s & \text{if } \tau\geqslant 1 \end{Bmatrix}, \tag{21}$$

where

$$\tau \triangleq t/T_s. \tag{22}$$

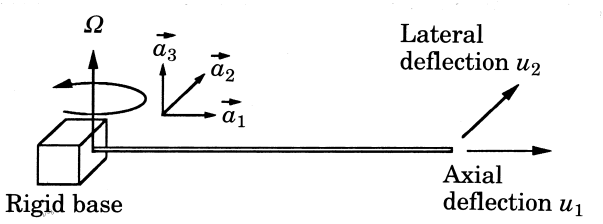

Figure 3. Abrupt planar spin-up motion of a cantilever beam. Mass per unit length $\rho = 550$ kg/m; Young's modulus $E = 6{\cdot}89\ \mathrm{E}\ 9\ \mathrm{N/m^2}$, length $L = 30{\cdot}5$ m, cross-sectional area $A = 9{\cdot}29\ \mathrm{E} - 2\ \mathrm{m^2}$, area moment of inertia $I = 7{\cdot}19\ \mathrm{E} - 4\ \mathrm{m^2}$, time constant $T_s = 1{\cdot}0$ s, steady state angular speed $\Omega_s = 0{\cdot}31$ rad/s.

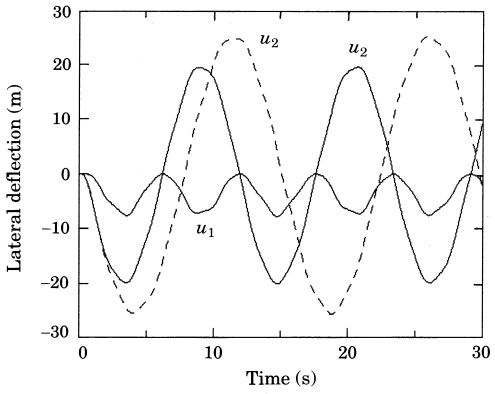

Figure 4. Simulation results for the abrupt spin-up example. ——, Present; ——, C.L.C.

Here Ω_s and T_s are the steady state angular speed and the time to reach the angular speed, respectively. This example was introduced and solved by the non-linear modelling method in reference [5]. All the numerical data are converted to SI units in this paper. The simulation results are shown in Figure 4. The axial and transverse tip deflections (denoted as u_1 and u_2) were obtained by using the present modelling method (solid lines) and the C.L.C. modelling method (dotted line). It is clearly shown that the two methods produce quite different numerical results. However, it is found that the results obtained by the present modelling method are almost identical to those obtained by the non-linear modelling method in reference [5]. The foreshortening effect (reduction of u_1 due to the change of lateral deflections u_2 or u_3) can be observed from the result obtained by the present modelling method. As the lateral deflection becomes large, large negative axial deflection results (as shown in Figure 4). As mentioned in section 2, u_1 can be determined numerically by using equation (4) once s, u_2 and u_3 have been obtained by numerical integration. It should be noted that the maximum lateral deflection in the plot is quite large. Thus, the present modelling method is as effective as the non-linear modelling method for solving large deflection problems of beams.

Another similar numerical example is shown in Figure 5. For this example, the prescribed base motion is smooth and is given as

$$\Omega = \begin{cases} \Omega_s[\tau - (1/2\pi)\sin(2\pi\tau)] & \text{if } 0 \leqslant \tau \leqslant 1 \\ \Omega_s & \text{if } \tau \geqslant \end{cases}, \tag{23}$$

where τ is defined same as in equation (22). This motion smoothly increases the angular speed until it reaches the steady state and the steady state angular speed is sustained. It is so smooth and slow that the lateral oscillation after reaching the steady state remains quite small. In Figure 6 are shown the simulation results (lateral deflections) by the present

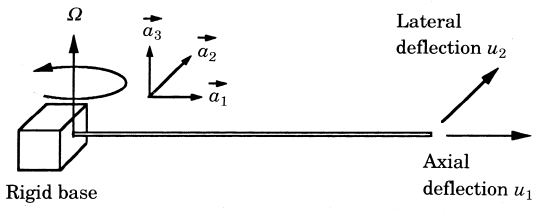

Figure 5. Smooth planar spin-up motion of a cantilever beam. Mass per unit length $P = 1{\cdot}2$ kg/m, Young's modulus $E = 7{\cdot}0$ E 10 N/m^2, length $L = 10$ m, cross-sectional area $A = 4{\cdot}0$ E $-$ 4 m^2, area moment of inertia $I = 2{\cdot}0$ E $-$ 7 m^4, time constant $T_s = 120$ s, steady state angular speed $\Omega_s = 6{\cdot}0$ rad/s.

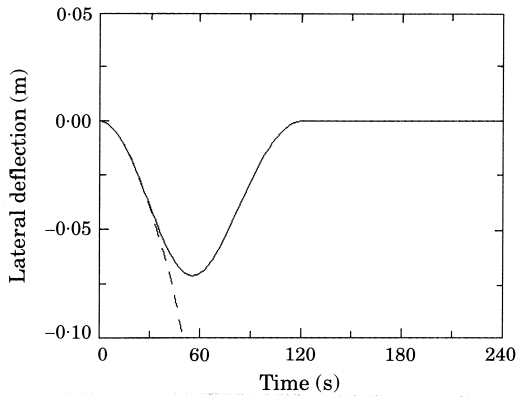

Figure 6. Simulation results for the smooth spin-up example. ——, Present; – – –, C.L.C.

modelling method (solid line) and the C.L.C. modelling method (dotted line). The figure shows that even for the relatively small deflection case the C.L.C. modelling method fails to provide reasonable results. It is often believed that the C.L.C. modelling method can be safely used unless the displacement becomes relatively large. This example shows that such an idea is not always correct. The effective range of the C.L.C. modelling method can be identified only by inspecting the factors involved in the motion induced stiffness terms (second and third terms in square brackets of equations (19) and (20)). The terms should not be ignored if they are significant enough in comparison with the elastic stiffness terms in the equations of motion, whereas the C.L.C. modelling method can be as effective as the present modelling method if they are relatively small.

For the purpose of exhibiting the three-dimensional capability of the formulation derived in this paper, a problem of a rotating cantilever beam attached to a rigid base with a taper angle α has been solved. The prescribed function in equation (23) is used for the numerical analysis. With the numerical data given in Figure 7, simulation results were obtained and are plotted in Figure 8. The results show the difference between the results of the present modelling method (solid line) and those of the C.L.C. modelling method (dotted line). The steady state lateral deflection u_2 does not converge to zero since the centrifugal inertia force acting perpendicular to the rotating axis deforms the beam outwards. The magnitudes and frequencies of the steady state oscillation of u_3 obtained by the two modelling methods are also shown to be quite different from each other. The steady state deformed shape of the beam (in the plane of $\check{a}_1$ and $\check{a}_2$) is shown in Figure 9.

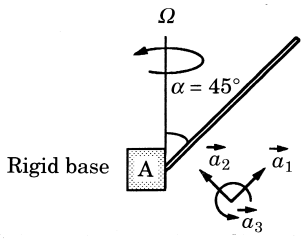

Figure 7. Three-dimensional motion example of a cantilever beam. Mass per unit length $P = 1{\cdot}2$ kg/m, Young's modulus $E = 7$ E 10 N/m^2, length $L = 10$ m, cross-sectional area $A = 4$ E $-$ 4 m^2, area moments of inertia $I_{yy} = 2{\cdot}0$ E $-$ 7 m^4 and $I_{zz} = 4{\cdot}0$ E $-$ 7 m^4, time constant $T_s = 1{\cdot}5$ s, steady state angular speed $\Omega_s = 3$ rad/s.

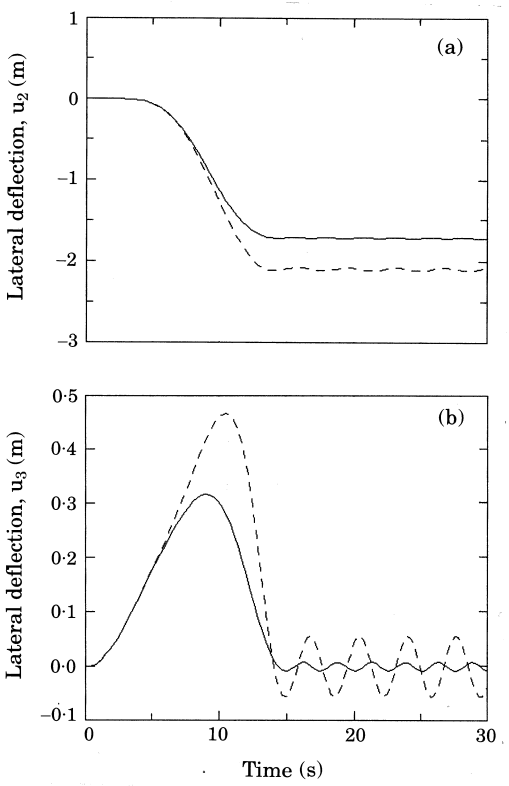

Figure 8. Simulation results for the three dimensional motion example. (a) Lateral deflection u_2; (b) lateral deflection u_3. ——, Present; ——, C.L.C.

6. ANALOGY STUDY

With the results obtained in the previous section, the following questions may be raised. Why does the C.L.C. modelling method lack proper stiffness variation terms? How can the problem of the C.L.C. modelling method be resolved? How is the stiffness variation effect captured by the present modelling method? Does the choice of the deformation variable play a role in obtaining a proper modelling method? What is the key ingredient of the non-linear modelling method? These questions need to be addressed to provide better insight into dynamic modelling of flexible structures undergoing large overall motions.

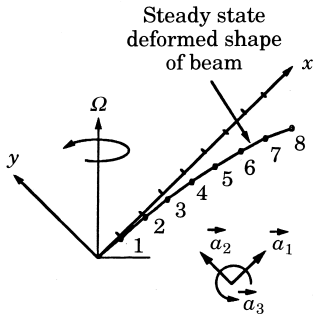

Location of the points		
NB	x	y
1	1·25	−0·05
2	2·49	−0·17
3	3·73	−0·36
4	4·96	−0·59
5	6·18	−0·86
6	7·40	−1·14
7	8·61	−1·42
8	9·83	−1·72

Figure 9. The steady state deformed shape of the 3-D example.

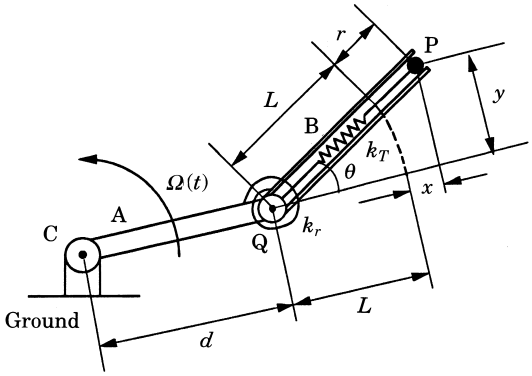

Figure 10. A discrete system analogous to a rotating cantilever beam. Link A is rigid; inner wall of B is frictionless.

Due to the complexities involved in structural theories, it may not be easy to obtain proper answers to the questions raised in the previous paragraph. Therefore, a simple discrete system which is analogous to a flexible structure undergoing large overall motion was devised. Due to the analogy, the discrete system exhibits characteristic behavior similar to that of flexible structures. Since the discrete system possesses only two degrees of freedom, the exact equations of motion can be easily derived and solved numerically. Furthermore, the mathematical modelling analogy (between the discrete system and continuous flexible structures) enables one to obtain the answers to the previously raised questions. The mathematical models developed for the discrete system have their analogous counterparts in the continuous modelling methods. Therefore, the conclusions drawn from the study of discrete system can shed light on dynamic modelling strategy for flexible structures.

The discrete mechanical system depicted in Figure 10 is representative of the class of problems of interest, in that it involves large overall motions as well as small elastic deformations. The system consists of the following elements: a rigid link A of the length d, attached to ground through a revolute joint at point C; a smooth massless tube B, connected to A via a revolute joint at point Q; a torsional spring of modulus k_r acting between A and B; a particle P, of mass m, which slides freely along the smooth inner wall of tube B; and a translational spring, of modulus k_T, which connects P to point Q. When the translational spring is undeformed, the distance between P and Q is denoted by the symbol L. The rotational motion of A, defined in terms of the magnitude Ω of its inertial angular velocity vector, is prescribed as a function of time. Thus, the system possesses two degrees of freedom and the equations of motion can be derived in terms of any two of the four variables θ, s, x and y, introduced in the figure. The symbol θ refers to the radian measure between the line of action of the translational spring force and the line extending through points C and Q. The stretch in the translational spring is represented by the symbol s, and the variables x and y refer to the axial and transverse displacements, respectively, of P relative to the line CQ. The rotational and translational springs are undeformed when $\theta = 0$ and $s = 0$, respectively. This model is similar to a rotating cantilever which exhibits both extensional and bending flexibility. The extensional and bending stiffnesses are represented by the translational and the rotational springs, respectively.

The main objective of the present section is to illustrate how different choices of deformation co-ordinates coupled with linearization result in different mathematical models which lead to radically different predictions of system behavior. This can provide

TABLE 1

Five mathematical models for the discrete system

NC set: fully non-linear in x and y:

$$m\ddot{x} - m\dot{\Omega}y - 2m\Omega\dot{y} - m\Omega^2(d + L + x) + \partial U_1/\partial x + \partial U_2/\partial x = 0,$$

$$m\ddot{y} + m\dot{\Omega}x + 2m\Omega\dot{x} - m\Omega^2 y + \partial U_1/\partial y + \partial U_2/\partial y = 0,$$

$$U_1 = \tfrac{1}{2}k_T\{[(L + x)^2 + y^2]^{1/2} - L\}^2, \qquad U_2 = \tfrac{1}{2}k_r[\tan^{-1}\{y/(L + x)\}]^2.$$

NP set: fully non-linear in s and θ:

$$m\ddot{s} + m\dot{\Omega}d\sin\theta - m(L + s)(\dot{\theta} + \Omega)^2 - md\Omega^2\cos\theta + \partial U_1/\partial s = 0,$$

$$(L + s)[m(L + s)\ddot{\theta} + m\dot{\Omega}(L + s + d\cos\theta) + 2m\dot{s}(\dot{\theta} + \Omega) + md\Omega^2\sin\theta] + \partial U_2/\partial\theta = 0,$$

$$U_1 = \tfrac{1}{2}k_T s^2, \qquad U_2 = \tfrac{1}{2}k_r\theta^2.$$

LC set: linear in x and y:

$$m\ddot{x} - m\dot{\Omega}y - 2m\Omega\dot{y} - m\Omega^2(d + L + x) + k_T x = 0,$$

$$m\ddot{y} + m\dot{\Omega}x + 2m\Omega\dot{x} + (-m\Omega^2 + k_r/L^2)y = 0,$$

$$U_1 = \tfrac{1}{2}k_T x^2, \qquad U_2 = \tfrac{1}{2}k_r(y/L)^2.$$

LP set: linear in s and θ:

$$m\ddot{s} + m\dot{\Omega}d\theta - 2mL\Omega\dot{\theta} - m\Omega^2(d + L + s) + k_T s = 0,$$

$$mL^2\ddot{\theta} + m\dot{\Omega}L(L + d) + m\dot{\Omega}(2L + d)s + 2mL\Omega\dot{s} + (mdL\Omega^2 + k_r)\theta = 0,$$

$$U_1 = \tfrac{1}{2}k_T s^2, \qquad U_2 = \tfrac{1}{2}k_r\theta^2.$$

NS set: non-linear in x and y, up to second degree stretch related to k_T:

$$m\ddot{x} - m\dot{\Omega}y - 2m\Omega\dot{y} - m\Omega^2(d + L + x) + k_T x + \tfrac{1}{2}k_T(y^2/L) = 0,$$

$$m\ddot{y} + m\dot{\Omega}x + 2m\Omega\dot{x} + (-m\Omega^2 + k_r/L^2)y + k_T(xy/L) + k_T(y^3/2L^2) = 0,$$

$$U_1 = \tfrac{1}{2}k_T(x + y^2/2L)^2, \qquad U_2 = \tfrac{1}{2}k_r(y/L)^2.$$

important insight into any modelling methods intended for the treatment of motion-induced structural stiffness variations. The two sets of co-ordinates to be studied in this example are the Cartesian co-ordinate set x and y and the non-Cartesian (polar) co-ordinate set s and θ.

In Table 1 are listed five sets of dynamic equations relevant to the system represented in Figure 10. The table also contains five sets of strain energy expressions used to obtain the five dynamical equation sets. U_1 and U_2 represent the strain energies stored in the translational and the torsional springs, respectively.

The first two sets of equations, labelled NC (non-linear Cartesian) and NP (non-linear polar), represent the fully non-linear equations of motion expressed in terms of (x, y) and (s, θ), respectively. One can easily demonstrate their mathematical equivalence. Thus, when numerical simulations are performed, the two models always produce equivalent results. Actually, any fully non-linear exact model can produce equivalent results.

Now, if straightforward mathematical linearization of set NC in x and y and set NP in s and θ is performed (all terms of degree two and higher in x, $\dot{x}$, y, $\dot{y}$, s, $\dot{s}$, θ and $\dot{\theta}$ are dropped), one obtains the third and fourth equation sets, respectively. These two sets of equations, labelled LC (linear Cartesian) and LP (linear polar) are similar in form, with one crucial difference. The second equation in set LP contains a stiffness term which increases in magnitude with increasing Ω, thus exhibiting the well known centrifugal stiffening effect. In contrast to this, the second equation of set LC involves a stiffness term

which decreases in magnitude with increasing Ω, thereby effectively softening the rotational spring. This is in direct conflict with experimentally observed behaviors. As will be shown later in this section, the solution of set LP matches closely that of its non-linear counterpart NP for a wide range of Ω values; such is not the case, however, for LC and NC. The important fact is that the two linearization procedures based on different co-ordinate sets results in two qualitatively different mathematical models. It is possible to obtain such a result since the exact models (NC or NP) are linearized only in co-ordinates, but not in Ω, which is not generally small.

Since the development of equation set LC involves no linearization in inertia force contributions, the problem of the LC set should be caused by dropping non-linear terms of the active force in the equations of motion. In Figure 11(a) are shown the centrifugal force $\vec{F}_c$ and the translational spring force $\vec{F}_k$ acting on the particle P. Also shown in the axial and transverse directional components of the two forces, $\vec{F}_{cx}$, $\vec{F}_{cy}$ $\vec{F}_{kx}$ and $\vec{F}_{ky}$. Note that the transverse direction component of the centrifugal force has a destabilizing effect on the particle P (''destabilizing'' simply means that the force component pushes the particle away from the undeformed position: i.e., $x = y = s = \theta = 0$). This leads to the

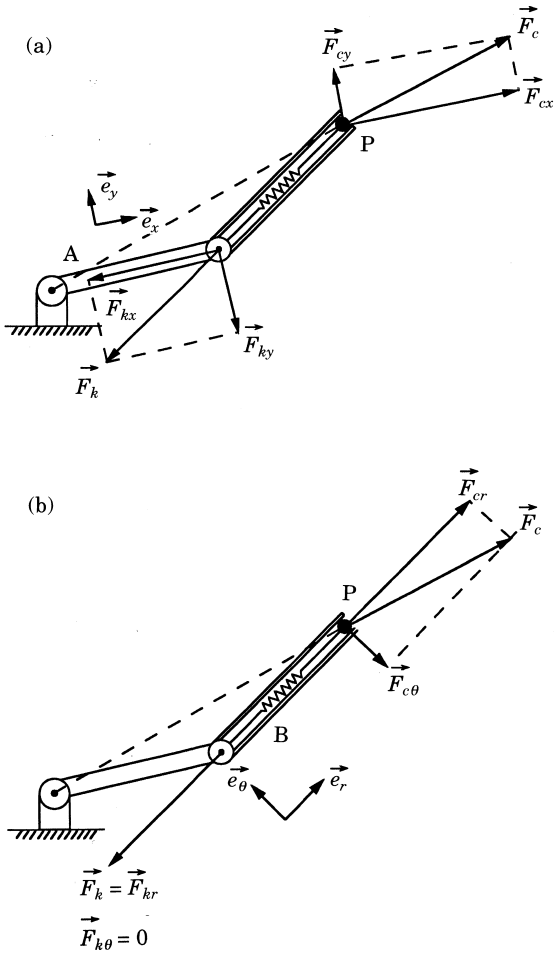

Figure 11. The resolution of centrifugal and translational spring forces in Cartesian and polar components. (a) Resolution of forces in Cartesian (axial and transverse) components ($\check{e}_x$ and $\check{e}_y$ are unit vectors fixed in A); (b) resolution of forces in polar (radial and tangential) components ($\check{e}_r$ and $\check{e}_\theta$ are unit vectors fixed in B).

softening effect on the rotational spring in the LC models. Thus, the destabilizing motion-induced stiffness term $-m\Omega^2 y$ appears in the LC set. However, the actual problem of the LC model lies in the linearization of the translational spring force. Actually, the same destabilizing effect is included in the NC set. However, in the NC set, the destabilizing effect is compensated by non-linear terms in the translational spring force. The translational spring force is dependent on the extension in the spring. Hence, in the mathematical expression for the spring force, system co-ordinates appear at least to the first degree (linearly) or higher. When this spring force is then resolved into two components, parallel to $\check{e}_x$ and $\check{e}_y$ (see the sketch) respectively, the mathematical expression for the $\check{e}_y$ component of the force will be of the second degree or higher in the system co-ordinates due to the trigonometric sine of the angle between $\vec{F}_k$ and $\vec{F}_{kx}$. $\vec{F}_{ky}$ is, therefore, not included in the LC model. The truncation of $\vec{F}_{ky}$ would not be significant if $\vec{F}_{ky}$ were small compared to other linear terms in the equations of motion. Unfortunately, $\vec{F}_{ky}$ is significant, since it involves the translational spring coefficient k_T, which is very large compared to any other parameters of the system. For instance, k_T is much larger than k_r since the discrete system is devised to imitate a flexible structure in which the stretching stiffness is much larger than the bending stiffness.

Unlike the equation set LC, the equation set LP involves no linearization of the active force contributions. It involves linearization only in the inertia force contributions. Therefore the LP set does not have the problem linearizing the translational spring force since it expresses the force in an exact linear form. The linearization of the inertia force, however, does not cause any serious problems in the LP set. Since the inertia force has an expression of zero degree and higher, the LP set contains all the zero and first degree terms of inertia force with the linearization. Furthermore, the magnitude of the parameter (m) involved in the inertia force is not very large compared to other parameters of system. Therefore, the truncation of the inertia force terms which are second degree and higher does not affect the fidelity of the LP set (to the NP set). In Figure 11(b) are shown the centrifugal force $\vec{F}_c$ and the translational spring force $\vec{F}_k$ acting on the particle P. Also shown are the radial and tangential direction components, $\vec{F}_{cs}$, $\vec{F}_{c\theta}$, $\vec{F}_{ks}$ and $\vec{F}_{k\theta}$. Unlike the transverse direction component of the centrifugal force in Figure 11(a), the tangential direction component in Figure 11(b) has a stabilizing effect. The stabilizing term $mdL\Omega^2 y$ appears in the LP set. Therefore, the combination of linearized forces (by $\vec{F}_{c\theta}$ and $\vec{F}_{k\theta}$) has a stabilizing effect. This leads to the fundamental difference (stiffness variations due to large overall motion) between the LC and LP models.

Since the failure of the LC model results from the truncation of non-linear terms in the active force contribution, one can overcome the difficulty by keeping all non-linear active terms (as in the NC set). However, is it necessary to keep all the non-linear terms to develop an accurate model? To find the answer to this question, the NS set was generated as follows. The stretch length of the translational spring is approximated up to second degree in terms of x and y and retained in the strain energy expression associated with the translational spring. The effectiveness of this set, in comparison with NC set, was then evaluated by using numerical simulations in order to determine whether such a model does indeed capture the motion-induced stiffness variation effect.

It is worthwhile to note the analogies between the discrete models and the structural modelling method discussed in the previous sections. The fully non-linear NC model is analogous to the non-linear modelling method (introduced in reference [5]), which is based on fully non-linear exact strain measures for flexible structures. The LC model is analogous to the C.L.C. modelling method, since they both employ Cartesian deformation measures and linear quadratic strain energy expressions. The LP model is analogous to the modelling method developed in this paper, since they are both based on non-Cartesian deformation

TABLE 2

Data of the discrete system used for numerical simulations

Notation	Numerical data	Description
m	1 kg	Mass of particle P
L	1 m	Unstretched length of translational spring
d	1 m	Distance from C to Q
k_T	600 000 N/m	Translational spring stiffness
k_r	300 Nm/rad	Torsional spring stiffness
Ω_s	10 rad/s	Steady state angular speed of spin-up case 1
Ω_s	20 rad/s	Steady state angular speed of spin-up case 2
T_s	1 s	Steady-state time constant for spin-up cases
$x(0)$	0 m	Initial value of x
$y(0)$	0 m	Initial value of y
$\dot{x}(0)$	0 m/s	Initial value of $\dot{x}$
$\dot{y}(0)$	0 m/s	Initial value of $\dot{y}$
t	0–2 s	Simulation time interval

measures with which the exact strain energy (for stretching) can be expressed in quadratic forms. Lastly, the NS model is analogous to the non-linear modelling method based on von Kármán strain measures (see, for instance, reference [11]) since they are both based on the second degree strain measures expressed in Cartesian variables.

Simulations were performed by using the parameters listed in Table 2. For the large overall motion (represented by Ω) of the system, a spin-up function (given in equation (23))

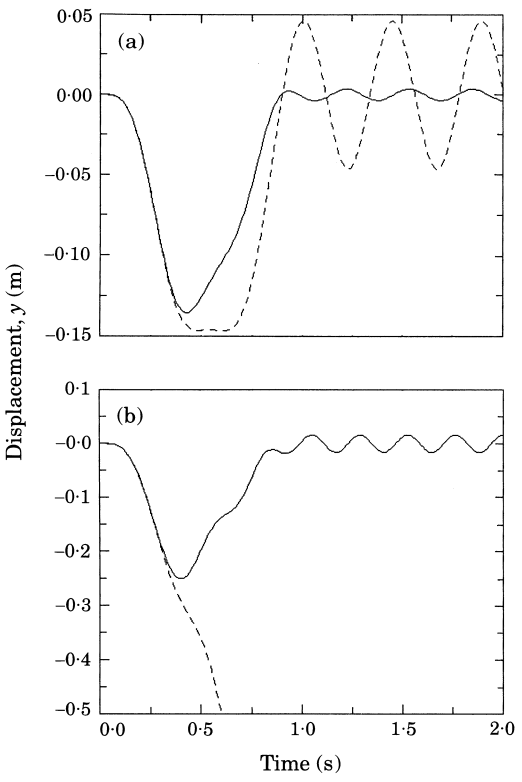

Figure 12. A comparison of the numerical results obtained by using the NC (——) and LC (– – –) models. (a) Angular speed $\Omega_s = 10$ rad/s; (b) angular speed $\Omega_s = 20$ rad/s.

was used. Since the spin-up function varies with time, it is quite effective in representing general cases of overall motions.

In Figures 12 and 13 is provided a qualitative idea of the fidelity of the linear equation sets LC and LP relative to their non-linear counterparts NC and NP. The lateral displacements y are plotted in the figures. In Figure 12 it is illustrated how poorly the solution of the LC set approximates that of NC. For the slower spin rate, $\Omega_s = 10$ rad/s, the errors are substantial. With the faster spin rate, $\Omega_s = 20$ rad/s, the linear equations incorrectly predict an unbounded response. The former response (with $\Omega_s = 10$ rad/s) is actually more disturbing than the latter (with $\Omega_s = 20$ rad/s), because the former response might appear reasonable in the absence of the correct response while the latter response is obviously in conflict with observed physical behavior. Figure 13, on the other hand, provides a glimpse of the impressive accuracy of the linear equation LP set in tracking the true solution even at high spin rates. For convenience of comparison, output results of all models are converted to the transverse displacement y. For instance, once s and θ had been obtained numerically in the LP set, y was calculated by using the trigonometric relation.

Additional simulations using the NS set were performed. The results are depicted in Figure 14. In each plot, the solid line represents the solution obtained by using the NC equation set and the dashed curve represents the solution obtained by using the NS equation set. As shown in the plot, the two curves are close to each other. Note that, however, the numerical results given by the NS equation set are no better than those given by the LP equation set, despite the additional effort of computation for high degree terms. If non-linear terms based on third or fourth degree stretch (or strain) are kept in the

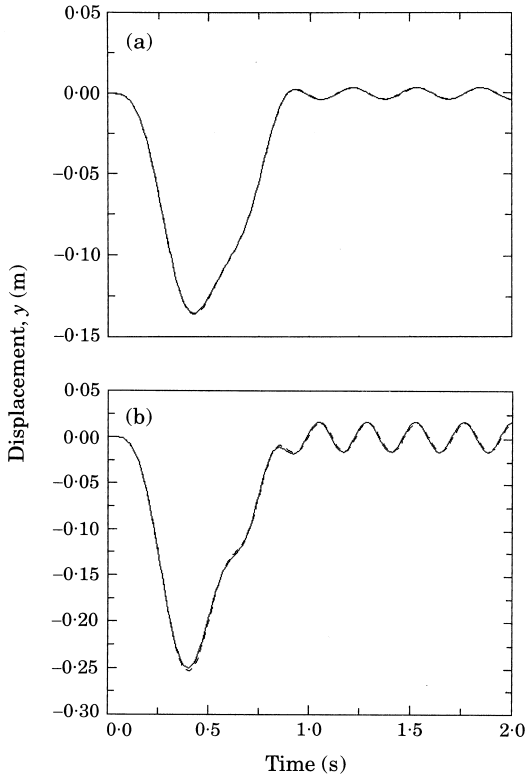

Figure 13. A comparison of the numerical results obtained by using the NP (——) and LP (– – –) models. (a) Angular speed $\Omega_s = 10$ rad/s; (b) angular speed $\Omega_s = 20$ rad/s.

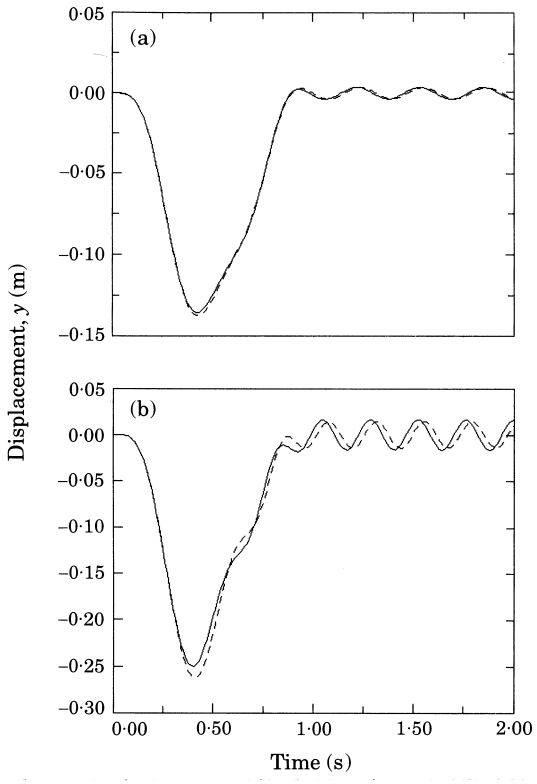

Figure 14. A comparison of the numerical results obtained by using the NC (——) and NS (– – –) models. (a) Angular speed $\Omega_s = 10$ rad/s; (b) angular speed $\Omega_s = 20$ rad/s.

equations of motion, the accuracy of the mathematical model will be improved. However, such models are not investigated here, since the counterparts (structural modelling) are not as meaningful as the von Kármán modelling (counterpart for the NS set) is.

Through the introduction and analysis of a simple discrete system, a number of important modelling issues such as motion-induced stiffness variations, their contribution to linear and non-linear equations of motion, their dependence on co-ordinate choice, and the influence of linearization procedures in accounting for such effects have been investigated. If one chooses a special set of deformation variables such that the strain energy of the structure is accurately characterized in a quadratic form in these variables, then it is possible to develop differential equations of motion which are totally linear in the deformation variables and yet still exhibit proper stiffness variations. This is clearly shown by the performance of the LP set. This is the approach taken in the modelling method developed in this paper, wherein the strain energy of the 3-D beam is expressed in a quadratic form by using the stretch variable of the beam. If one chooses the Cartesian set of deformation variables, the stiffness variation due to large overall motion cannot be properly predicted by a linear model. This is shown by the performance of the LC set. The counterpart (the C.L.C. modelling method) has shown spurious performances. If proper motion-induced stiffness variation is to be accommodated, at least up to second degree terms in the stretch strain should be retained. This is shown by the performance of the NS set. This is consistent with the results of the non-linear modelling method [11] based on von Kármán strain measures.

7. CONCLUSIONS

The present paper mainly serves to propose an accurate linear modelling method for flexible beams undergoing large overall motion and concomitant small linear elastic deformation. The crucial part of the present modelling method is the introduction of a stretch deformation variable by which the strain energy function can be expressed in a quadratic form (effectively resulting in linear generalized active forces in the equations of motion). In this modelling method, motion-induced stiffness variations are captured accurately and expressed in analytical forms in which large overall motion component functions are explicitly shown. This enables one to predict easily the relation between the amount of stiffness variations and large overall motions. By observing the stiffness variation terms shown in the equations of motion (these terms are absent in the equations of motion given by the C.L.C. modelling method), one may determine the range of validity of the C.L.C. modelling method. In other words, if the stiffness variation terms are small compared to the rest of the terms in the equations of motion, the C.L.C. modelling method may provide reasonable simulation results.

ACKNOWLEDGMENT

This work has been partially supported by the Korea Ministry of Education through Mechanical Engineering Research Fund (ME93-D-12), for which the authors are grateful.

REFERENCES

1. P. W. Likins and H. K. Bouvier 1971 *Astronautics and Aeronautics* **9**(5), 64–71. Attitude control of non-rigid spacecraft.
2. J. Y. L. Ho 1977 *Journal of Spacecraft and Rockets* **14**, 102–110. Direct path method for flexible multibody spacecraft dynamics.
3. C. S. Bodley, A. D. Devers, A. C. Park and H. P. Frisch 1978 *NASA Technical Paper* 1219 **1 & 2**. A digital computer program for the dynamic interaction simulation of controls and structure (DISCOS).
4. W. Hurty, J. Collins and G. Hart 1971 *Computers and Structures* **1**, 535–563. Dynamic analysis of large structures by modal synthesis techniques.
5. E. R. Christensen and S. W. Lee 1986 *Computers and Structures* **23**, 819–829. Nonlinear finite element modeling of the dynamics of unrestrained flexible structures.
6. J. C. Simo and L. Vu-Quoc 1986 *Journal of Applied Mechanics* **53**, 849–863. On the dynamics of flexible beams under large overall motions—the plane case: part I and part II.
7. T. Belytschko and B. Hsieh 1973 *International Journal of Numerical Methods in Engineering* **26**, 255–271. Nonlinear transient finite element analysis with convected coordinates.
8. W. J. Haering, R. R. Ryan and R. A. Scott 1992 33*rd Structures*, *Structural Dynamics*, *and Material Conference*, *Dallas*, *Texas*, *AIAA* 92-1162. A new flexible body dynamic formulation for beam structures undergoing large overall motion.
9. T. R. Kane, R. R. Ryan and A. K. Banerjee 1987 *Journal of Guidance*, *Control*, *and Dynamics* **10**(2), 139–151. Dynamics of a cantilever beam attached to a moving base.
10. R. R. Ryan 1986 *Ph.D. Dissertation*, *Stanford University*. Flexibility modeling method in multibody dynamics.
11. H. H. Yoo 1989 *Ph.D. Dissertation*, *The University of Michigan at Ann Arbor*. Dynamic modeling of flexible bodies in multibody systems.